DOI: 10.26599/FSHW.2025.9250826

Contents lists available at SciOpen

Food Science and Human Wellness

journal homepage: https://www.sciopen.com/journal/2097-0765

China Food Publishing Co.

Cyanidin-3-O-Glucoside Ameliorated Hepatic Steatosis in AGEs-rich MCD Diet Induced NAFLD Mice Model *via* Inhibiting Endoplasmic Reticulum Stress

Xiaoyu Liu [a], Yangming He [a], Xia Li [a], Xu Wang [b], Weibin Bai [a], Xinwei Jiang [a*]

[a] *Department of Food Science and Engineering, Institute of Science and Technology, Jinan University, Guangzhou, 510632, China*

[b] *Department of Clinical Nutrition, Guangdong Provincial People's Hospital (Guangdong Academy of Medical Sciences), Southern Medical University, Guangzhou, 510080, China*

ABSTRACT: Non-alcoholic fatty liver disease (NAFLD) could be worsened by endogenous and exogenous advanced glycation end products (AGEs). This study investigated how exogenous AGEs exacerbate NAFLD and whether cyanidin-3-O-glucoside (C3G) as an anthocyanin could mitigate liver damage. Mice were fed with baked methionine-choline deficient (MCD) diet and treated with low or high-dose C3G gavage for six weeks. Baked MCD diet induced severe steatosis and inflammation, while C3G, particularly at high doses, reduced lipid droplet accumulation and hepatic inflammation. Proteomics revealed C3G modulated lipid metabolism, mitochondrial function, and endoplasmic reticulum pathways, and suppressed lipid synthesis enzymes such as CD36, ACC, FASN and FABP4. These findings highlight anthocyanins' protective role in NAFLD by targeting lipid synthesis pathways, offering insights for dietary interventions and functional food development to combat metabolic liver disorders.

Keywords: anthocyanins, advanced glycation end products, NAFLD, AGEs, steatosis, inflammation

1. Introduction

Certain contaminants or harmful substances in foods can promote the occurrence and progression of non-alcoholic fatty liver disease (NAFLD). The specific pathogenesis of NAFLD is associated with imbalances in liver insulin resistance, leptin resistance, oxidative stress, and inflammation, and disturbances in hepatocyte lipid transport, synthesis, and hydrolysis[1]. However, recent researches indicate a close correlation between advanced glycation end products (AGEs) and fibrosis development in NAFLD, suggesting AGEs as a potential novel target for preventing liver fibrosis[2].

AGEs result from non-enzymatic reactions between glucose or fructose and amines, amino acids, and proteins, forming linear and cross-linked adducts through oxidative processes[3]. While endogenous AGEs are naturally produced in the body generally at low levels, they significantly elevate in various disease processes. In western diet treated mice models, higher level of AGEs was detected in organs. Particularly in patients with metabolic syndrome, disrupted glucose metabolism leads to slow reactions between reducing sugars and amino acids or proteins, generating AGEs. Elevated blood glucose levels in the body can lead to more than

***Corresponding author**
jiangxinwei@jnu.edu.cn

Received 30 May 2025
Received in revised from 1 July 2025
Accepted 25 July 2025

threefold accumulation of AGEs in organs such as the kidneys, lens of the eye, liver, and brain[3]. Furthermore, AGEs are found in commonly consumed foods, such as baked ham, bread, and other high-temperature baked or grilled foods. Additionally, some mild, low-temperature processes during the production and storage of items like milk, fruit juice, and beer can lead to the Maillard reaction, producing AGEs[4]. To date, over 20 types of AGEs have been identified in animal tissue proteins, with Nε-carboxymethyl-lysine (CML) and Nε-carboxyethyl-lysine (CEL) being the predominant forms. While high-temperature processed foods constitute a major source of daily AGEs intake, direct evidence linking high-temperature processed foods to the development of NAFLD remains insufficient, and the underlying mechanisms require clarification[5].

Anthocyanins, a class of naturally occurring flavonoids, widely distributed in fruits, vegetables and some dark-color cereals. Epidemiological studies suggest that anthocyanin-rich diets play a critical role in mitigating degenerative and chronic diseases, attributed to their potent antioxidant and anti-inflammatory properties. Emerging evidence highlights anthocyanins regulate lipid metabolism and combat hepatic steatosis[6]. Whereas, anthocyanins suppress fatty acid synthesis by modulating acetyl-CoA carboxylase (ACC), sterol regulatory element-binding protein-1 (SREBP-1), and fatty acid synthase (FAS), while enhancing fatty acid oxidation *via* peroxisome proliferator-activated receptor alpha (PPARα) and carnitine palmitoyltransferase-1 (CPT1) activation[7]. Cyanidin-3-glucoside (C3G) as a monomer of anthocyanins reduces hepatic triglyceride accumulation and steatosis by inhibiting c-Jun N-terminal kinase (JNK) activation. C3G enhances glutathione synthesis *via* phosphorylation of cAMP-response element binding protein (CREB) and glutamate-cysteine ligase catalytic subunit (Gclc), countering hyperglycemia-induced oxidative liver injury[8]. However, it can not illustrate clearly whether the protective mechanism of anthocyanins is related to AGEs pathway or not.

To clearly investigate the role of anthocyanins on food-source AGEs induced liver injury, we applied methionine-choline-deficient (MCD) diet to establish a NAFLD model, which will not induce insulin resistance and generate endogenous AGE*s in vivo*. Furthermore, the MCD diet was baked under high-temperature to let the mice exposed to exogenous AGEs, then the mice model was intervened with different doses of C3G. We aim to investigate whether anthocyanins can effectively attenuate hepatic lipid deposition and exert hepatoprotective effects through AGEs-related pathways.

2. Materials and methods

2.1 Materials and reagents

MCD and standard growth diet AIN-93G were purchased from Research Diets (New Brunswick, USA). The baking of MCD diet was based on previous research[9], performed at 160℃ for 20 min in an oven. C3G was extracted from the peel of the black soy bean, according to our previous method, and the purity was about 96%[10].

2.2 Experimental animals

Male C57BL/6 mice, 16 weeks old with an average weight exceeded 28 g, were obtained from the Guangdong Provincial Medical Animal Experiment Center. Mice were housed in SPF rooms at the Experimental Animal Center of Jinan University, with a 12-hour light-dark cycle, temperature maintained at 22℃-26℃, and relative humidity between 60% and 80%. They were provided *ad libitum* access to food and water. The experimental protocol was approved by the Ethics Committee of Jinan University and carried out in accordance with relevant guidelines (IACUC Issue No: 20210709-010). After the quarantine period, 45 mice were then graded by weight and randomly assigned to five groups, with 9 mice each: mice were fed with AIN-93M standard diet for the control group, and MCD diet (MCD), or baked MCD diet model group (BMCD) for the model and intervention groups. The baked MCD diet with the gavage treatment of C3G with a dosage 60 mg/kg·BW was marked as BMCD+LC3G group, and baked MCD diet with the gavage treatment of C3G 120 mg/kg·BW was marked as BMCD+HC3G group. Meantime, the control group, MCD group and the BMCD group were administrated with normal saline. Mice were *ad libitum* feeding, and their weight changes were recorded weekly, with feeding performance noted every two days. After six weeks of modeling, mice were euthanized.

2.3 Samples collection

Mice were fasted but allowed water for 12 hours prior to euthanasia. Anesthetization was operated by intraperitoneal injection of 1% pentobarbital sodium (600 mg/kg·BW). Blood was collected from the eye socket, and the organs were weighed and recorded. Liver tissue sample was immediately placed in 2.5% glutaraldehyde fixative for transmission electron microscopy examination. A portion of the liver tissue samples were fixed in 10% paraformaldehyde for 48 hours for paraffin embedding, and another portion was placed in OCT embedding medium, frozen in liquid nitrogen, and stored at -80℃ for frozen section preparation. The remaining liver tissue was divided into multiple aliquots and stored at -80℃ for future use. After keeping at room temperature for 30 minutes, blood samples were centrifuged at 4℃ and 3000 r/min for 15 minutes to separate serum, which was stored at -80℃ for later testing.

2.4 CML level examination

CML as a typical AGE was measured in diets and mice liver after been sacrificed. ELISA kit for measuring the CML level was purchased from Cloud-Clone Corp (Houston, USA) and the operation followed the guidance of the manual book. The results of the CML level in animal diet was presented as μg/mg diet, the level in liver sample was presented as ng/mg protein.

2.5 H&E staining and sirus red staining

Hematoxylin staining solution and eosin staining solution were obtained from Xiuwei Chemical (Guangzhou, China). Sirus red was obtained from Han Guang Chemical Reagent (Shanghai, China). Fast green was purchased from Sigma-Aldrich (USA). Picric acid was obtained from Guangzhou Chemical Reagent Factory (Guangzhou, China). For the H&E staining, slides were stained with hematoxylin for 2 minutes, rinsed with tap water for 5 minutes, and then stained with eosin for 5 seconds. For the sirus red

staining, slides were stained with picric acid for 5 minutes, rinsed in running water for 5 minutes, stained with sirus red for 1 hour, rinsed twice with 0.5% acetic acid, air-dried, re-stained with fast green for 1 minute. The slides were rinsed with distilled water, dehydrated in gradient ethanol and xylene, and sealed with neutral resin. Photos of five random fields were taken under microscope with 200× magnification.

2.6 Mouse NAFLD Activity Score and Fibrosis Evaluation

Under light microscopy, hepatic tissue stained with H&E was evaluated according to the NAFLD activity score (NAS) standards with five aspects: steatosis (0-3), steatosis location (0-3), lobular inflammation (0-3), Chronic portal inflammation (0-2), and ballooning (0-2)[11]. Fibrosis severity was scored with 0-3. Scoring was performed according to an internationally recognized protocol, as outlined in Table 1. The NAS ≥5 will be considered as NASH period.

Table 1. Histology by NAS Scoring system

Steatosis	<5%	5-33%	34-66%	>66%
	0	1	2	3
Steatosis location	Zone 3	Zone 1	Azonal	Panancinar
	0	1	2	3
Lobular inflammation	None	<2	2-4	>4
	0	1	2	3
Chronic portal inflammation	None	Mild	>Mild	
	0	1	2	
Liver cell Ballooning	None	Few	Many	
	0	1	2	
Fibrosis	None	Perisinusoidal or Periportal	Perisinusoidal and Periportal	Bridging
	0	1	2	3

2.7 Cytokines detection in serum

The levels of IL-1α, IL-1β, IL-10, IL-17A and IL-6 in serum were measured using the ProcartaPlex multiplex analysis system (eBioscience, Thermo Fisher, USA). Briefly, microspheres were incubated with samples, washed, detection antibodies were added, then the plate was washed again, SA-PE was added, and the plate was shaken at room temperature in an oscillating shaker at 500 r/min for 30 minutes. The plate was washed again, and 120 μL of reading buffer was added to each well. After shaking at 500 r/min for 5 minutes, the plate was read using the Luminex 200 high-throughput protein chip detector. Concentrations were calculated using a five-parameter nonlinear regression method based on the standard curve. MCP-1 and TNF-α were measured by ELISA kit (eBioscience, Thermo Fisher, USA) according to the manual book.

2.8 Proteomics profiling

Proteins were labeled and identified using the iTRAQ labeling technique, and the relative expression levels of proteins in the samples were calculated. Briefly, 4 liver samples in each group were randomly chosen, and the protein samples were extracted, and BCA method was applied for quantification. Protein samples were added with buffer, DTT, IAA solution to reduce disulfide bonds Enzymatic Digestion, and used trypsin to digest protein into peptides. Dissolve the sample TEAB Buffer, and incubated with iTRAQ reagent to label the samples. Peptide separation was performed using an Agilent 1100 HPLC system. The collected

fractions were centrifuged, dried, and prepared for LC-MS analysis. Later, triple TOF LC-MS/MS analysis was performed. Results of conventional bioinformatics analysis of differential proteins encompass three aspects: Gene Ontology (GO) enrichment analysis, KEGG Pathway analysis, and Protein-Protein Interaction (PPI) analysis.

2.9 Biochemical indicator determination in liver tissue and serum

Triglyceride (TG) assay kit was purchased from Applygen Technology (Beijing, China). Aspartate aminotransferase (AST) assay kit and alanine aminotransferase (ALT) assay kit were obtained from Nanjing Jiancheng Bioengineering Institute (Nanjing, China). MDA, SOD was obtained from Beyotime Biotechnology (Shanghai, China). These biochemical indicators were measured following the specific procedures as directed in the kit manuals.

2.10 Measurement of mitochondria in liver tissue

Liver tissue was fixated with glutaraldehyde for transmission electron microscopy examination. The hepatocytes were examined under the 1.2k zoom and 5k zoom for the observation of cell status and organelle morphology. The mitochondrial membrane potential of fresh liver tissue was evaluated by extracting mitochondria using a commercial kit (Beyotime Biotechnology, Shanghai, China) and assessing the production of JC-1 red fluorescent dimers. The intensity of red and green fluorescence was measured at wavelengths Ex/Em-580/590 and Ex/Em-510/527, respectively, using a fluorescence microplate reader, and their fluorescence intensity ratio was calculated.

2.11 Quantitative Real-Time PCR

The specific procedure primarily adhered to the instructions provided by Takara (Dalian, China), summarized as follows. Liver tissue was homogenized in Trizol using a homogenizer, and total RNA was extracted through chloroform and alcohol precipitation steps. Subsequently, reverse transcription was conducted to generate cDNA using a reverse transcription kit. Amplification was performed using a SYBR green kit, and based on CT values, the amplification status of each sample in various groups was calculated with $2^{-\Delta\Delta CT}$ to infer the relative mRNA expression levels of different samples. Primer sequences for RT-qPCR are shown in Table 2.

Table 2. Primer sequences for RT-qPCR

Gene	Orientation	Primer sequences (5'-3')
Bcl2 (Bcl-2)	Forward	ATGCCTTTGTGGAACTATATGGC
	Reverse	GGTATGCACCCAGAGTGATGC
Bax (Bax)	Forward	AGACAGGGGCCTTTTTGCTAC
	Reverse	AATTCGCCGGAGACACTCG
Hspa5 (GRP78)	Forward	ACTTGGGGACCACCTATTCCT
	Reverse	ATCGCCAATCAGACGCTCC
Xbp1 (XBP-1)	Forward	AGCTTTTACGGGAGAAAACTCAC
	Reverse	CCTCTGGAACCTCGTCAGGA
Ocln (occludin)	Forward	TTGAAAGTCCACCTCCTTACAGA
	Reverse	CCGGATAAAAAGAGTACGCTGG
Tjp1 (ZO-1)	Forward	GCCGCTAAGAGCACAGCAA
	Reverse	TCCCCACTCTGAAAATGAGGA

Mtor (mTOR)	Forward	GAGCTGGTGGTGCTGTTCTT
	Reverse	CAGCAGCAGGTAGGTGATGA
Ddit3 (CHOP)	Forward	AAGCCTGGTATGAGGATCTGC
	Reverse	TTCCTGGGGATGAGATATAGGTG

2.12 Western blot analysis

Liver tissue was homogenized in RIPA buffer with protease and phosphatase inhibitors. The homogenates were centrifuged at 14,000×g for 15 min at 4℃, and the protein concentration of supernatant was measured using the BCA assay, and the protein concentration of each sample were adjusted to the same. 20 μg of protein per sample underwent 10% SDS-PAGE, then transferred to PVDF membranes. Membranes were blocked with 5% non-fat dry milk in TBST for 1 h, and incubated overnight at 4℃ with primary antibodies (target proteins ACC, FASN, FABP4, CD36, ATGL, CPT-1 were diluted with 1:1000, and β-actin 1:2000). After washing, HRP-conjugated secondary antibodies (1:5000) were applied for 1 h. Protein bands were visualized *via* ECL and analyzed with ImageJ. Data were normalized to β-actin and presented as relative fold changes against the control group.

2.13 Data processing and analysis

All experimental data underwent statistical analysis using SPSS 16.0 software. Experimental results were presented as mean ± standard error. Between-group comparisons were subjected to one-way analysis of variance (ANOVA), followed by Bonferroni's post multiple comparisons test. Mann-Whitney U test was utilized to assess NAS scores, with $P < 0.05$ considered statistically significant. Bar graphs were generated using GraphPad Prism 9.3.

3. Results

3.1 Basic evaluation on diets and animal status

After the diet was baked, the level of CML in MCD diet shown a little higher than the standard diet, while BMCD group was almost 3 times higher than unbaked groups (Fig. 1A). Following a 6-week intervention, 4 mice in the BCMD group and 1 mouse in MCD group died with extreme thinness. The body weights of mice in both the MCD and BMCD groups significantly decreased by approximately 30% compared to the control group, and there was no significant difference between the BMCD and MCD groups. C3G treatment has no impact on the weight of mice, but the mice in these two groups were with better living state (Fig. 1B). Measurement of liver weights revealed a reduction in the MCD and BMCD groups compared to the control group. BMCD group showed a significant decrease of the liver weight, approximately half than the control group. C3G treatment has no effect on liver weight either (Fig. 1C). However, when liver weight ratio was calculated, the BMCD group exhibited a slight increase with no significance compared to the control group, and C3G treatment showed a little decrease compared to the BMCD group (Fig. 1D). The liver of mice in the MCD and BMCD groups displayed a yellowish, non-glossy appearance with clear distribution of lipid droplets, but the treatment of C3G showed much normal appearance in liver with some dark color in the liver lobule. CML level in the liver of BMCD group was significantly elevated compared to the control group,

while the treatment of C3G has no influence on the liver CML level (Fig. 1E). To further evaluate the liver status, oxidative stress was measured. MDA as an important indicator of lipid peroxidation, was significantly elevated in both MCD and BMCD groups, while treatment with high dose of C3G reduced MCD level significantly (Fig. 1F). As to the SOD level, it has no significant change in every group (Fig. 1G).

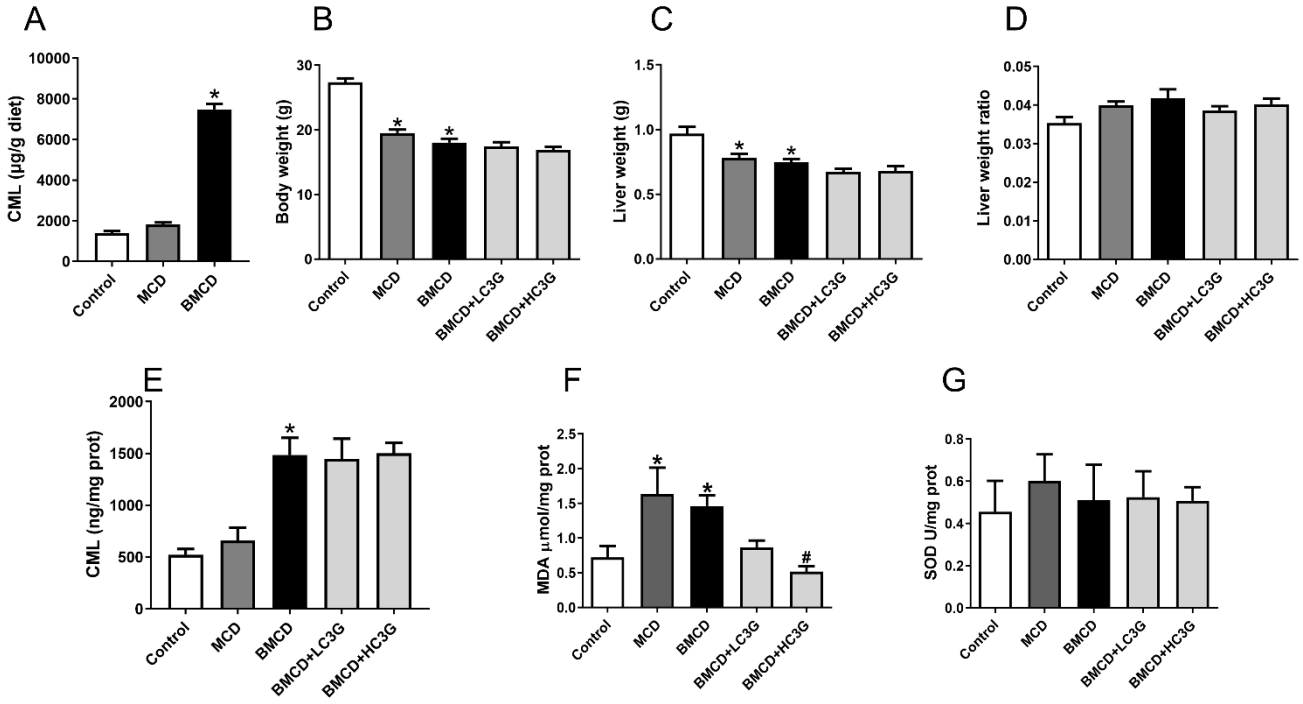

Fig. 1. Mice treated with different diets for 6 weeks. CML levels in animal diet were measured by ELISA (A), body weight was shown (B), liver weight was shown (C), and liver/body weight ratio (D) was calculated. CML level in liver was analyzed (E). MDA and SOD level in liver tissue was measured (F&G). The results were expressed as mean ± SEM. When MCD group and BMCD group compared with control group, $^{*}P < 0.05$ was applied for the significant difference. When the BMCD+LC3G, BMCD+HC3G groups compared with BMCD group, $^{\#}P < 0.05$ showed the significant differences in groups.

3.2 Histological analysis of liver tissue

H&E staining of liver tissue revealed that numerous lipid vacuoles in the MCD group, predominantly of macrovesicular steatosis, located around the central vein, with sporadic diffuse distribution. In the BMCD group, lipid vacuoles were more extensive and widespread, including microvesicular steatosis. While treated with C3G, the hepatic tissue was exhibited with less steatosis and portal inflammatory region compared to the BMCD group (Fig. 2A). Sirius red staining indicated that the mice in the MCD and BMCD groups displayed mild collagen accumulation, signifying an early stage of hepatic inflammation and fibrosis. C3G treatment, especially the high dose has shown normal appearance of liver collagen distribution (Fig. 2B).

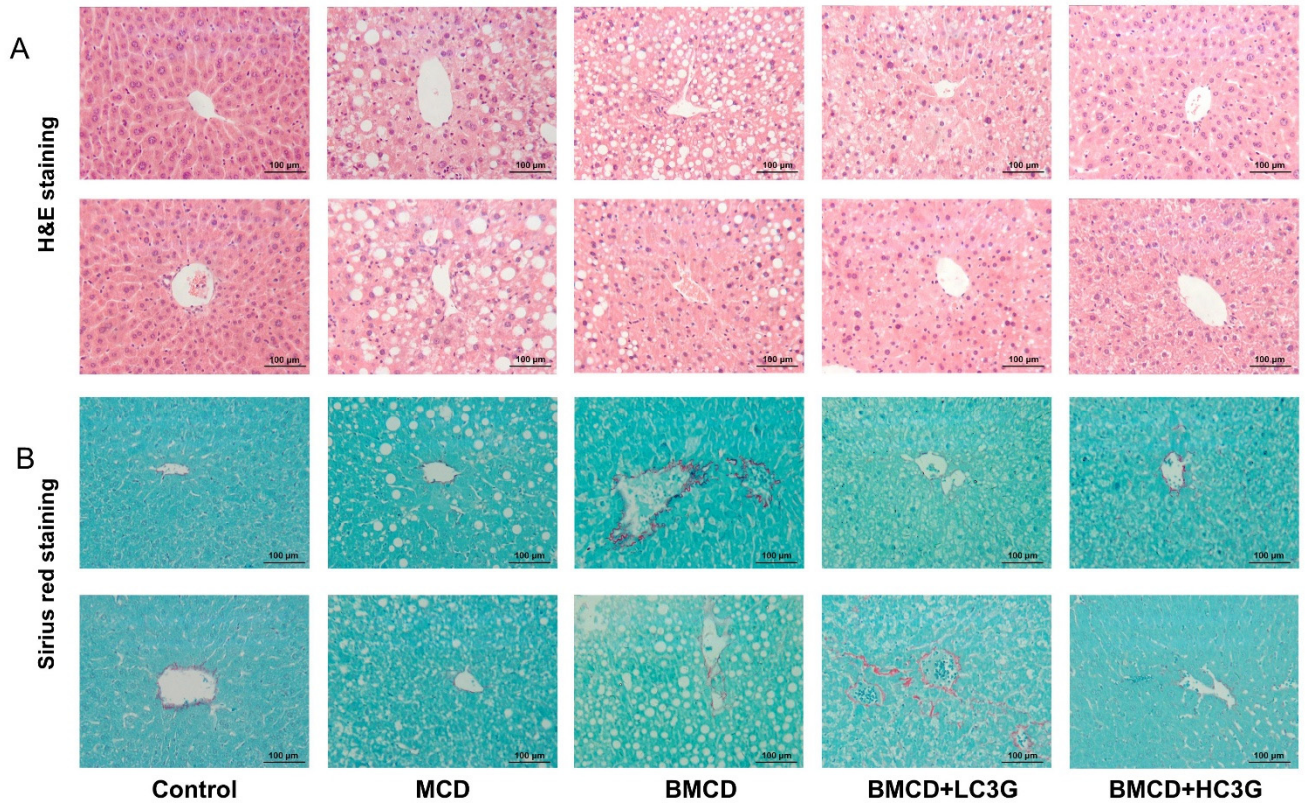

Fig. 2. Liver tissue histology was analyzed under light microscope, with a magnification of 200×, H&E staining (A), Sirius red staining (B).

3.3 Assessment of liver injury

Evaluation of liver tissue injury through multi-dimensional assessment of steatosis, inflammation, and ballooning by NAS scores for each group. Both the MCD and BMCD groups demonstrated significantly increased NAS scores compared to the control group, indicating mild-to-moderate fatty liver conditions. The average score of NAS in BMCD is above 5, showed a NASH status in this group. C3G treatment significantly reduced the NAS score, and the high dose almost led to the normal NAS level (Fig. 3A). When evaluating the fibrosis stage, MCD and BMCD group showed significant elevation, C3G treatment have shown no significant change (Fig. 3B).

Triglyceride content assessment by liver tissue homogenization indicated elevated TG levels in both MCD and BMCD groups compared to the control group, while significant decreased in the C3G treated groups (Fig. 3C). Evaluation of serum transaminase levels, ALT and AST, indicated a significant elevation in both MCD and BMCD groups compared to the control group. Additionally, the AST level in the BMCD group was higher than that in the MCD group. ALT and AST levels decreased with significance in C3G treated groups compared with the BMCD group, and higher dose of C3G treatment induced more decrease of ALT level (Fig. 3D&E). Elevated ALT levels are indicative of initial damage of hepatocytes, and the rise in AST levels suggests additional mitochondrial injury. As to the serum chemokine MCP-1 levels, they showed slight increases in model and treatment groups, which showed limited migration of inflammatory cells (Fig. 3F).

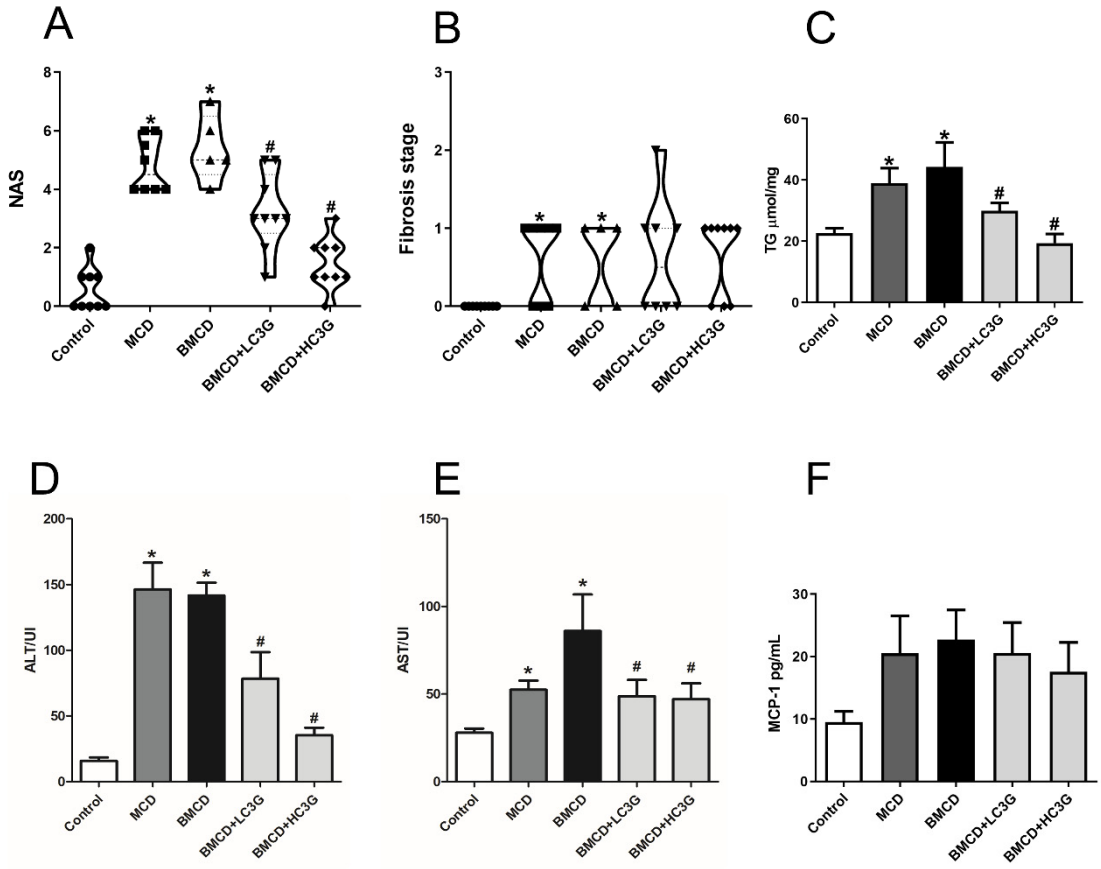

Fig. 3. Assessment of liver injury. NAS score was calculated in every mouse liver, based on the evaluation of steatosis, lobular inflammation, ballooning, and fibrosis severity (A). Liver fibrosis level was evaluated by fibrosis score (B). Liver TG level was measured (C), ALT and AST level in the serum were measured by the assay kit (D&E), and MCP-1 level in serum was measured by ELISA (F). The results were expressed as mean ± SEM. When MCD group and BMCD group compared with control group, $^{*}P < 0.05$ was applied for the significant difference. When the BMCD+LC3G, BMCD+HC3G groups compared with BMCD group, $^{\#}P < 0.05$ showed the significant differences in groups.

3.4 Measurement of inflammatory cytokines in serum

Utilizing ProcartaPlex high-throughput multiplex analysis, serum IL-1α, IL-1β, and IL-6 levels were significantly increased in both MCD and BMCD groups compared to the control group. Notably, IL-1β and IL-6 exhibited a more pronounced increase in the BMCD group, with IL-6 showing a remarkable 30-fold elevation compared to the control group. While C3G treatment significantly reduced these cytokines (Fig. 4A-C). IL-10 and IL-17A in MCD and BMCD groups showed no significant differences compared to the control group, while high dose C3G treatment reduced the IL-17A significantly (Fig. 4D&E). TNF-α is a pro-inflammatory cytokine secreted from liver, regulate the progression of inflammation. The increase of TNF-α in BMCD group was with a significant difference compared with the control group, and it was significantly reduced in C3G treated groups with dose-dependent manner (Fig. 4F).

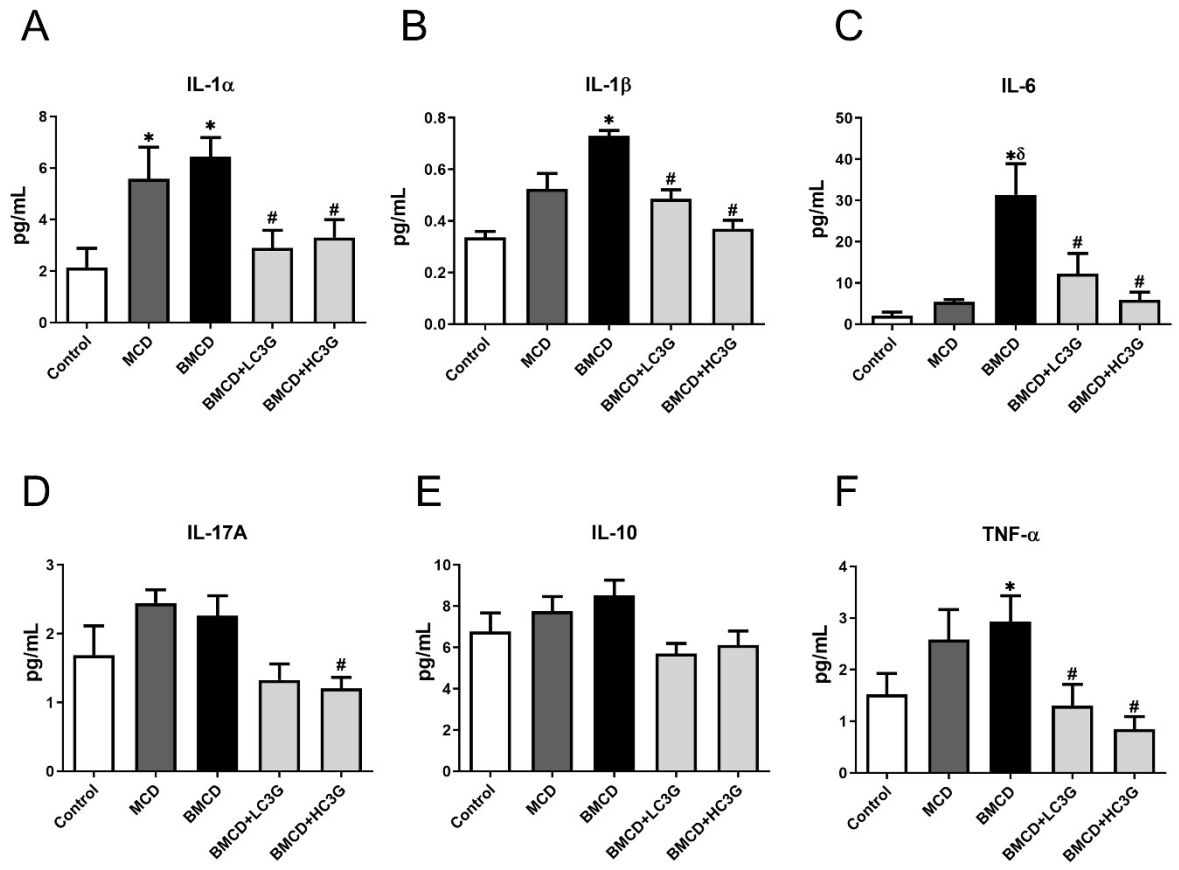

Fig. 4. Serum inflammatory cytokines were measured by ProcartaPlex multiplex analysis (A-F). The results were expressed as mean ± SEM. When MCD group and BMCD group compared with control group, $^{*}P < 0.05$ was applied for the significant difference. When the BMCD+LC3G, BMCD+HC3G groups compared with BMCD group, $^{\#}P < 0.05$ showed the significant differences in groups.

3.5 Quality control of liver tissue proteomics and the differential protein evaluation

Proteomics was conducted on liver tissue from all experimental groups. Firstly, the quality control parameters of the proteomics were performed. For high-resolution mass spectrometers, peptide-spectrum match (PSM) result showed the mass spectrometry error range is acceptable (Fig. 5A). For protein identification, the greater the number of spectra and the greater the number of peptides of the identified protein, the higher the reliability of the protein. About 68% of the proteins can have more than two spectra to support their identification, 59% of the proteins have 2 more unique peptide number to support (Fig.5 B&C). The identification reliability of the proteome is evaluated for false positives using the Target-decoy method. The protein identification threshold for this project is a false discovery rate (FDR) of less than 1%. The FDRs of both the spectra and the proteins are evaluated respectively, about 99.6% of the PSM FDR, and 95.3% of the Protein FDR was lower than 0.25%. (Fig. 5D&E).

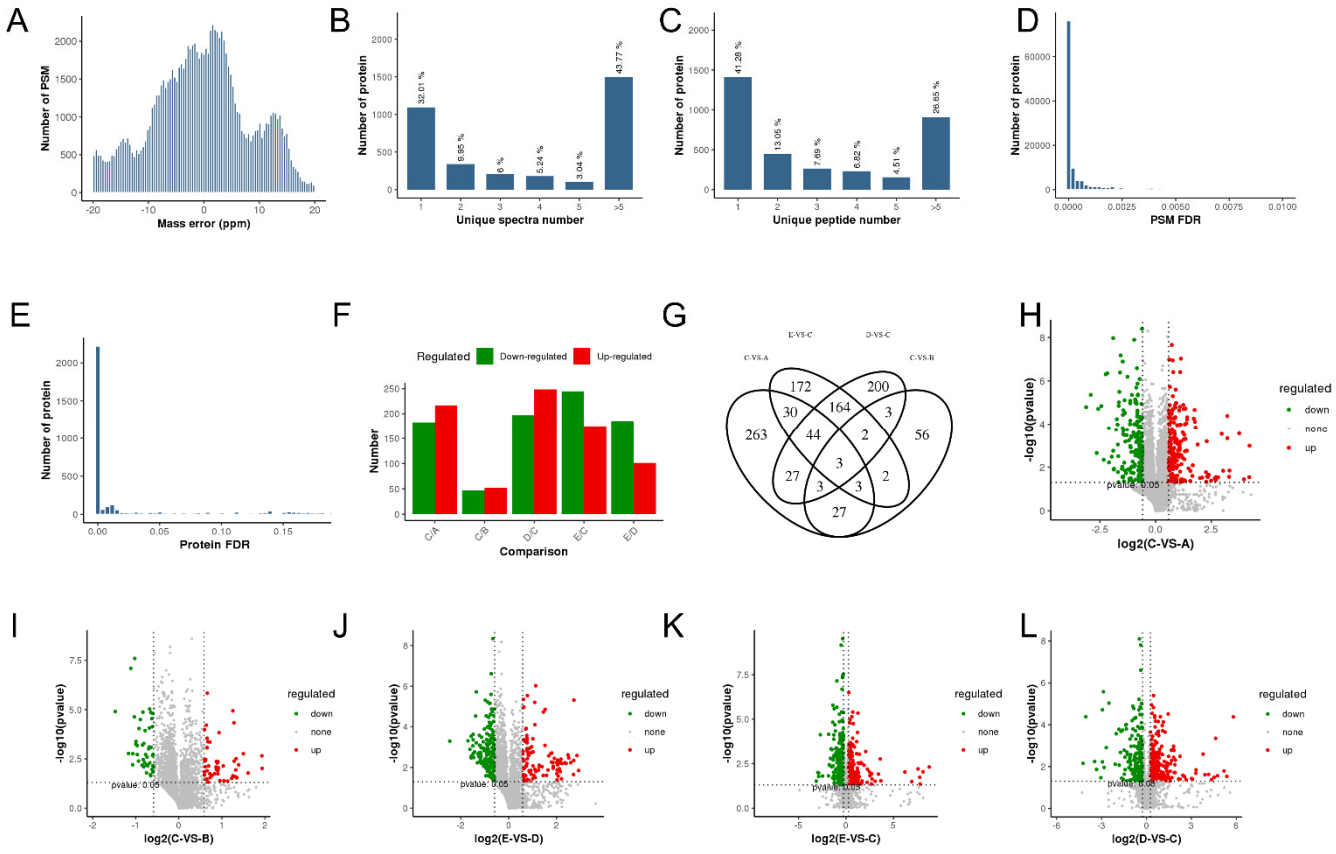

Fig. 5. Quality control of liver tissue proteomics and the differential protein evaluation. For high-resolution mass spectrometers, peptide-spectrum match (PSM) result showed the mass spectrometry error range (A), the number of spectra and the number of peptides of the identified protein (B&C), The FDRs of both the spectra and the proteins (D&E). The differentially expressed proteins (DEPs) were then conducted (F), the overlapping differential proteins (G), and the volcano plot evaluated (H-L).

The analysis of the differentially expressed proteins (DEPs) was then conducted. Using univariate analysis, proteins with a fold change (FC) greater than 1.5, that is, proteins upregulated to 1.5 times or more or downregulated to 0.67 times or less, and with a $P < 0.05$ obtained from the t-test statistics were screened out as DEPs. The differences in BMCD group compared to the control and MCD group, and the outcomes of C3G intervention compared with BMCD groups were our primary focus. As it is shown in Fig. 5F, more DEPs were detected in C (BMCD) vs. A (control) group, compared to the C (BMCD) vs. B (MCD) group. C3G treatment were shown as D (BMCD+LC3G) and E (BMCD+HC3G) groups, which could induce hundreds of DEPs (vs. BMCD group), and the different doses also have significant differences of DEPs (E vs. D). In Fig. 5G, the C vs. A group indicating the baking of MCD which contribute 400 differential proteins. The C vs. B group representing protein changes caused by baking, revealed 99 differential proteins, including 52 upregulated and 47 downregulated. The intersection between C vs. A and C vs. B showed 36 co-regulated proteins, demonstrating that baking indeed further influences the modeling efficacy of MCD. The E vs. C comparison contained 420 differential proteins, while D vs. C had 446. These two groups shared an intersection of 213 proteins, all attributable to C3G intervention. The overlapping differential proteins may result from different C3G administration doses (Fig. 5G). The volcano plot evaluated the fold change and statistical test for each

comparison group, which indicated the important impact of baking and exposure of AGEs, and the C3G treatment downregulated much more protein in higher dose (Fig. 5H-L).

3.6 Bioinformatic analyze of proteomics

Through GO analysis of the DEPs and hypergeometric testing of their associated GO terms, enriched GO entries were identified. The GO enrichment factor (RichFactor) refers to the ratio of the number of DEPs in a specific functional category to the total number of annotated proteins in that category. A higher RichFactor indicates a greater degree of enrichment. From different comparison groups, key pathways of interest were screened. As shown in Fig. 6A, the pathways significantly affected during baked MCD modeling included nutrient metabolism, response to extracellular stimuli, lipid metabolism, lipid binding, stress response, iron ion transport, and reactive oxygen species transport (C vs. A). When further evaluated the baking influence on mice liver, the DEPs in BMCD vs. MCD (C vs. B) were then analyzed. From Fig. 6B, it is evident that baking the MCD diet primarily influenced cellular structure, particularly involving ribosomes, especially mitochondrial ribosomes. Additionally, alterations were observed in RNA polymerase II transcription factor activity and sequence-specific DNA binding. Analysis of Fig. 6C revealed that low-dose C3G intervention modulated cellular metabolism, extracellular exosomes, extracellular vesicles, and membrane-associated intracellular organelles. While high-dose C3G notably improved intracellular membrane systems, organelle lumens, and extracellular exosomes (Fig. 6D). Thus, C3G plays a critical role in enhancing cellular membrane structure. By analyzing the subcellular localization of DEPs, we can further clarify the relationship between the effects of C3G and cellular functional structures. According to groups C (BMCD) vs. A (control), the NAFLD model primarily impacted subcellular components such as mitochondria, extracellular matrix, endoplasmic reticulum, and cytoskeleton (Fig. 6E). Notably, from the results of E vs. C, the C3G intervention exerted significant effects on mitochondria, extracellular matrix, and endoplasmic reticulum (Fig. 6F).

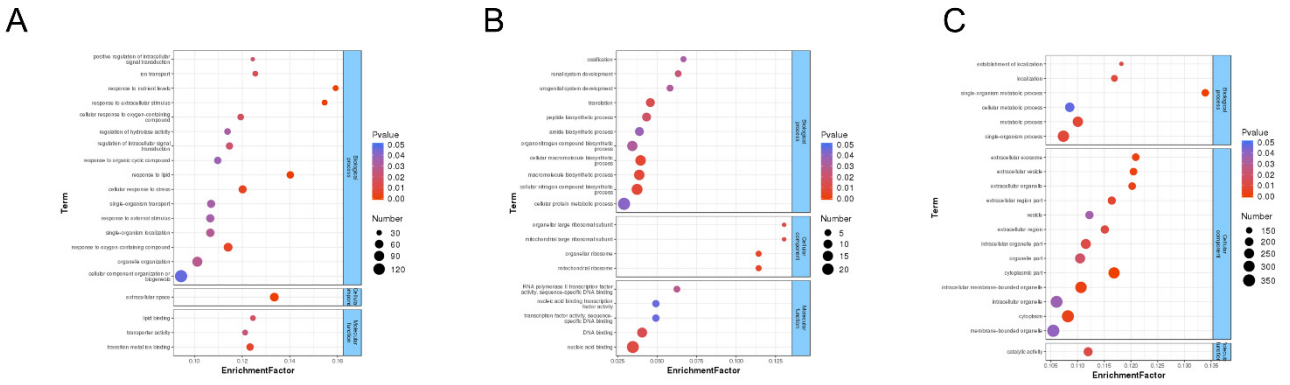

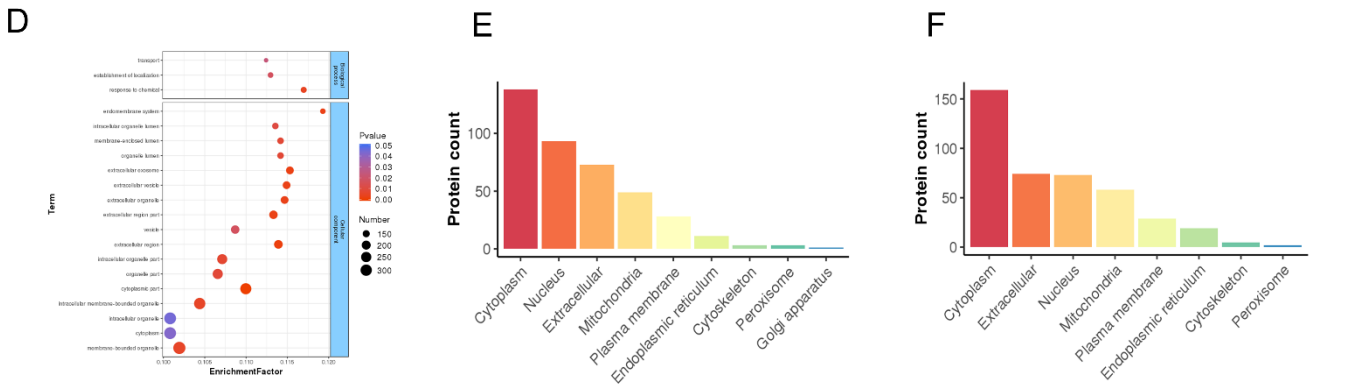

Fig. 6. Bioinformatic analyze of proteomics. GO analyses of different pathways, the BMCD vs. control group is shown in (A), the BMCD vs. MCD is shown in (B), is BMCD+LC3G vs. BMCD is shown in (C), BMCD+HC3G is shown in (D). The effects on cellular functional structures, the groups BMCD vs. control is shown in (E), BMCD+HC3G vs. BMCD is shown in (F).

3.7 Bioinformatic analyze of the DEPs with interests

The analysis of DEPs proved insufficient to precisely determine or narrow down the research scope. To identify the most significant pathways and target proteins associated with C3G effects, we conducted further data mining. Comparative analysis of protein level changes between groups revealed that comparisons against the BMCD control group (Group C) were critical, particularly the high-dose C3G treated group (E-vs.-C). Considering the potential false positives and uncertainties inherent in proteomic analysis, 420 DEPs were firstly cross-referenced from E-vs.-C with 1,337 proteins identified in D-vs.-C, excluding the proteins absent in D-vs.-C. This filtering yielded 332 conserved differential proteins in E-vs.-C. Subsequently, the proteins demonstrating consistent expression trends were screened between E-vs-C and D-vs-C. This rigorous selection process ultimately identified 76 proteins with coherent expression patterns across both intervention groups.

The DEPs of interest were further analyzed (as shown in Fig. 7). Pathways associated with C3G effects were identified through GO enrichment analysis of biological processes and cellular components, including organelle organization, glycosyl compound metabolic process, response to wounding, response to oxidative stress, organic acid metabolic process, and organonitrogen compound metabolic process (Fig. 7A). Extracellular exosome, vesicle, and extracellular membrane-bound organelles were highlighted as key cellular components (Fig. 7B). Influences of C3G on steroid hormone biosynthesis, selenocompound metabolism, and retinol metabolism were revealed by KEGG pathway analysis (Fig. 7C). Strong associations between C3G and immune-related pathways, such as systemic lupus erythematosus, as well as biosynthesis of unsaturated fatty acid, were demonstrated through protein-protein interaction (PPI) network analysis (Fig. 7D).

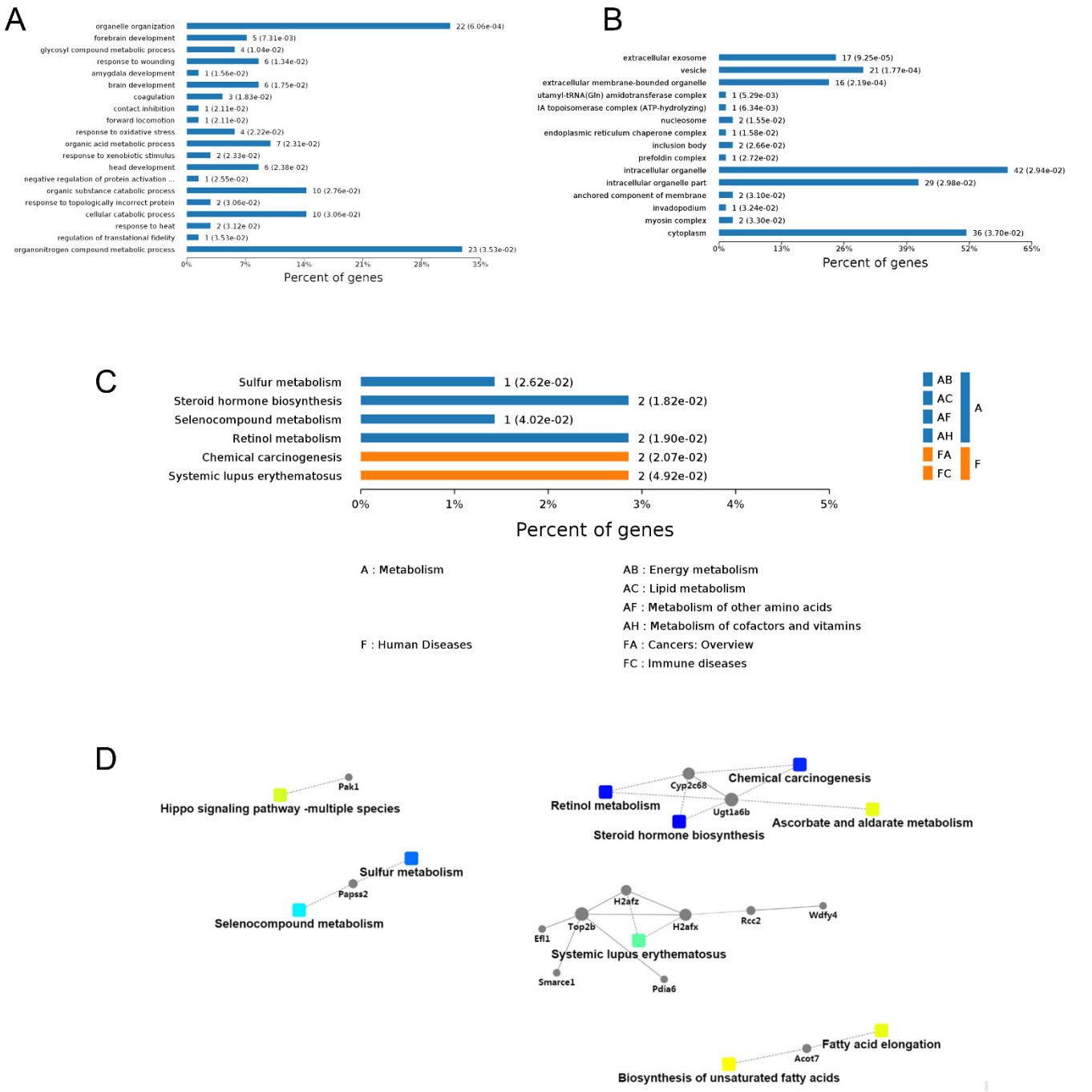

Fig. 7. Bioinformatic analyze of the DEPs with interests. After analyze the BMCD+HC3G vs. BMCD, the pathways associated with C3G effects were identified through GO enrichment analysis of the biological processes (A), and cellular components (B). KEGG pathway analysis (C), and protein-protein interaction (PPI) network analysis (D) are shown.

3.8 Further screen and bioinformatic analyze of the deps with interests

These DEPs with interests were subsequently subjected to further screening with A-vs.-C, during which proteins that had not exhibited significant alterations during the modeling were excluded, resulting in a final set of 20 proteins. Biological process analysis *via* GO enrichment revealed their functional associations: protein metabolic process (50%), organonitrogen compound metabolic process (50%), regulation of translational fidelity (5%), response to wounding (15%), carbohydrate metabolic process (15%), cellular amino acid metabolic process (10%), and organelle organization (35%) (Fig. 8A). Cellular component analysis identified key localization patterns: side of membrane (15%), glutamyl-tRNA (GIn) amidotransferase

complex (5%), anchored component of membrane (10%), mitochondrion (25%), mitochondrial envelope (15%), endoplasmic reticulum chaperone complex (5%), smooth muscle contractile fiber (5%), and CD40 receptor complexes (5%) (Fig. 8B). KEGG pathway analysis demonstrated significant impacts on arginine and proline metabolism (Fig. 8C). PPI network analysis revealed functional associations with cell adhesion molecules, leukocyte transendothelial migration, ribosome function, and protein processing in endoplasmic reticulum (Fig. 8D).

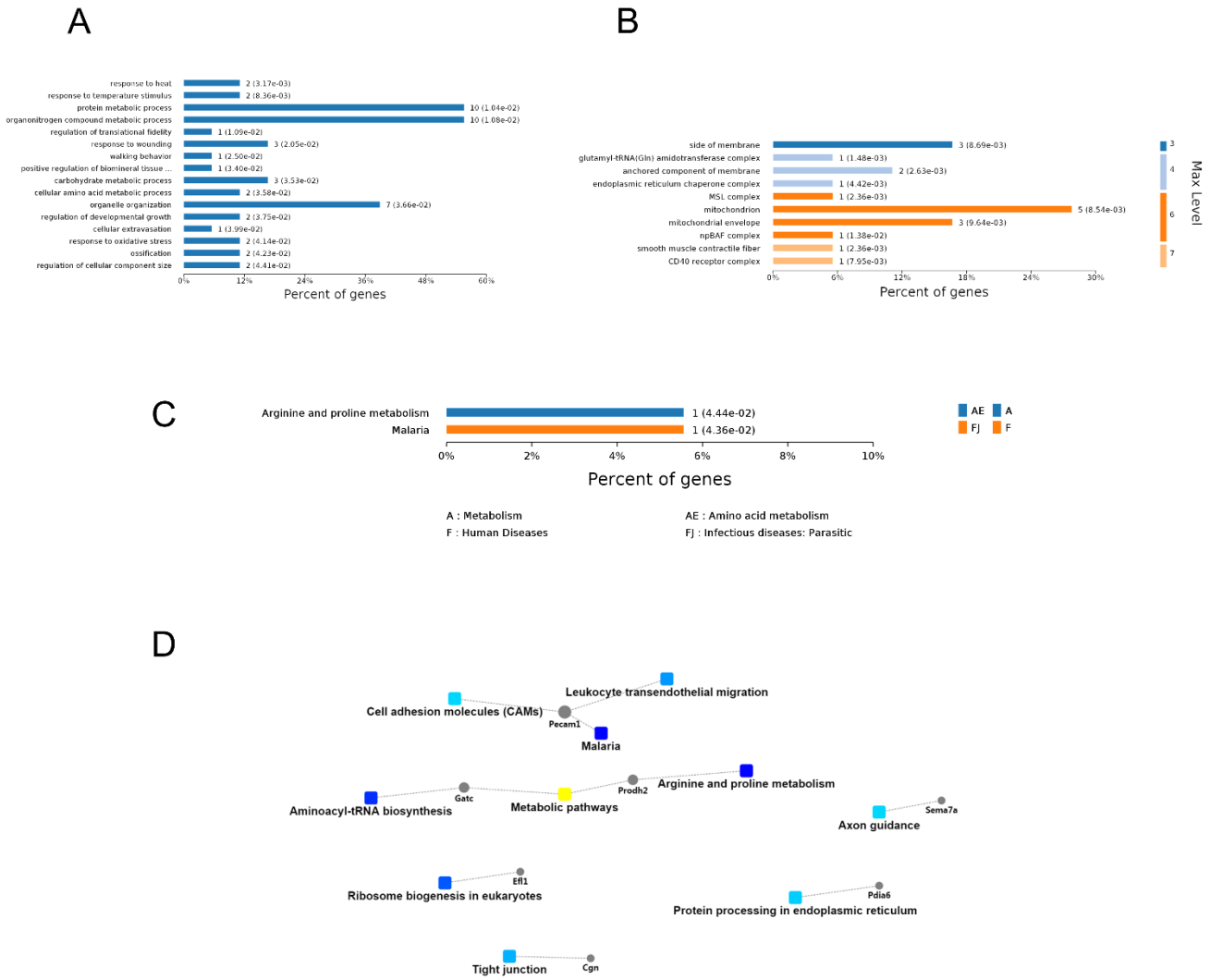

Fig. 8. Further screen and bioinformatic analyze of the 20 DEPs with interests. GO enrichment analysis of the biological processes (A), and cellular components (B). KEGG pathway analysis (C), and protein-protein interaction (PPI) network analysis (D) are shown.

3.9 Analysis of the status of hepatocyte organelles

Transmission electron microscopy observations of liver tissue, highlighted distribution of lipid droplets in hepatocytes, which is consistent to our previous test that BMCD group had more severe hepatic steatosis, while C3G treatment reduced the size and distribution of lipid droplets, especially the high dose C3G (Fig. 9A). Notably, the BMCD group exhibited nuclear shrinkage and less disrupted cristae, and with low matrix density in the cytoplasm in mitochondria. Normally, the rough endoplasmic reticulum and mitochondria are physically connected, while in BMCD group this combined situation reduced. The rough endoplasmic reticulum also showed expanded cisternal lumen, and loss of ribosomes, indicative of more pronounced cell

damage. While C3G treatment significantly reduced the number of abnormal mitochondria and rough endoplasmic reticulum, and increased the total number of mitochondria and the binding to the rough endoplasmic reticulum, especially in high dose C3G treated group.

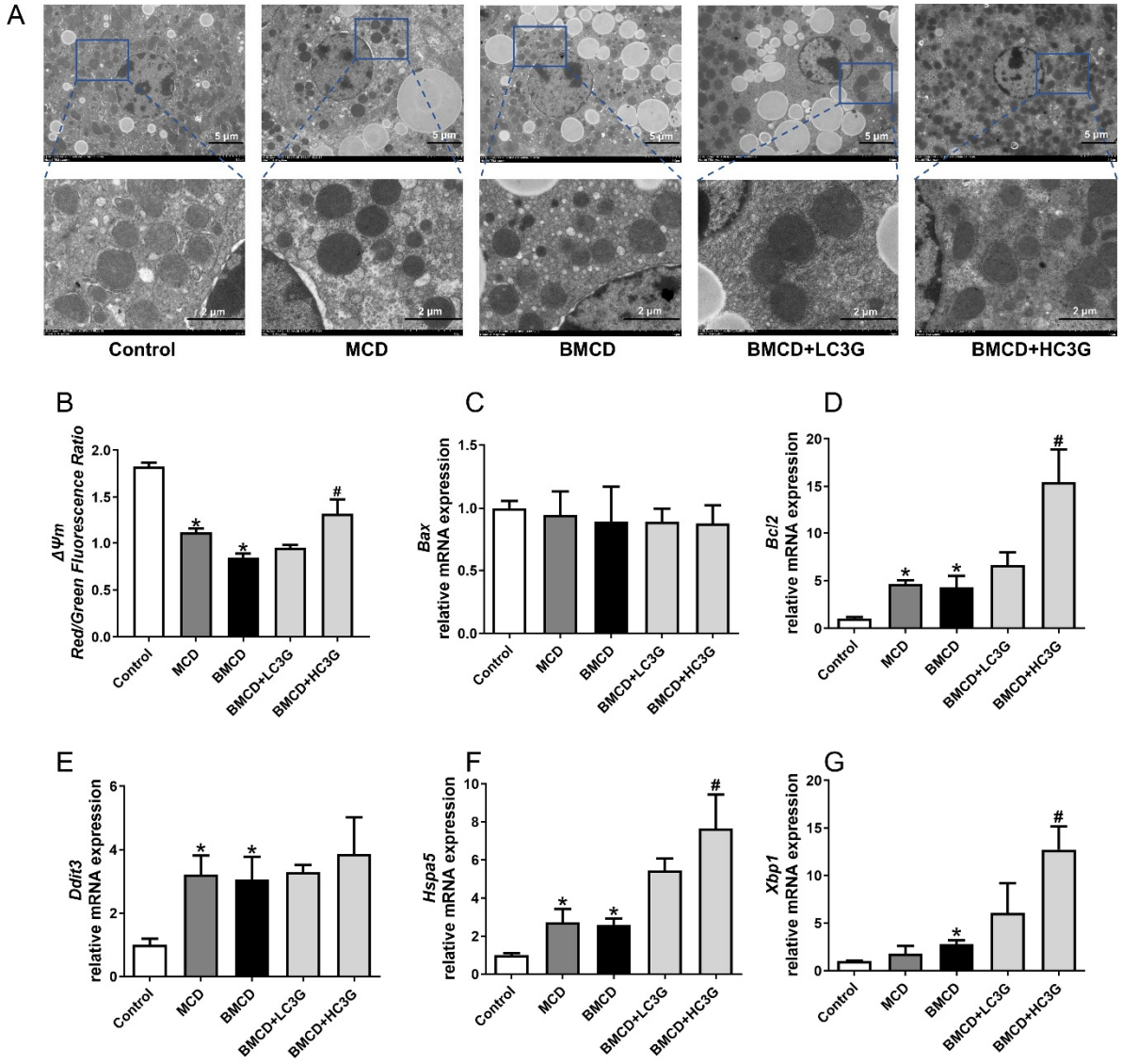

Fig. 9. Analysis of the status of hepatocyte organelles. Transmission electron microscopy observations of liver tissue (A), JC-1 fluorescence dye was used to measure the mitochondrial membrane potential (B), RT-qPCR were further applied to evaluate the mRNA level of crucial proteins related to mitochondria dysfunction and endoplasmic reticulum stress. Gene for Bax is shown as *Bax* (C), for Bcl-2 is shown as *Bcl2* (D), for CHOP is shown as *Ddit3* (E), for GRP78 is shown as *Hspa5* (F), for XBP-1 is shown as *Xbp1* (G). The results were expressed as mean ± SEM. When MCD group and BMCD group compared with control group, $^{*}P < 0.05$ was applied for the significant difference. When the BMCD+LC3G, BMCD+HC3G groups compared with BMCD group, $^{\#}P < 0.05$ showed the significant differences in groups.

JC-1 fluorescence dye was used to measure the mitochondrial membrane potential in the mitochondria isolated from liver tissue samples, and the red and green fluorescence were detected by the fluorescence-plate-reader. The relative ratio of red/green fluorescence in the MCD group was significantly lower than the control group, and in the BMCD group it further decreased, while C3G treatment significantly elevated the ratio, indicating the damage of mitochondrial membrane ameliorated (Fig. 9B). RT-qPCR were further applied to evaluate the mRNA level of crucial proteins related to mitochondria, endoplasmic reticulum (ER) and cell injury. The gene *Bax* in all groups showed no significant difference, while *Bcl2* increased a little

in the model groups, and increased dramatically in the BMCD+HC3G group (Fig. 9C&D). *Ddit3 as* the gene of CHOP, interacts with Bcl-2, and mediates with ER stress. The gene level of *Ddit3* increased in model groups and C3G treatment showed no effect on the expression (Fig. 9E). GRP78 and XBP-1 mRNA are *Hspa5* and *Xbp1* separately, and levels were significantly increased in BMCD group, and additionally increased in C3G treated groups, which indicated the early stage of ER stress and GRP78 might be stimulated to protect against the cell apoptosis (Fig. 9F&G).

3.10 C3G mediated the gene and protein expression related to lipid metabolism

Occludin and ZO-1 are two important proteins related to cell tight junctions which could mediate lipid metabolism and inflammatory cytokines release. The gene *Ocln* increased in model groups, and decreased in C3G treated groups (Fig. 10A). *Tjp1* gene expression increased in the model and intervention groups, and additionally raised in C3G treated groups, and the high dose C3G treatment had significant difference compared to BMCD group (Fig. 10B). mTOR as a key signaling mediator in NAFLD, which is closely related to ER stress, promote the fat syntheses and inhibit the fatty acid oxidation. The mRNA *Mtor* significantly elevated in BMCD group and dramatically decreased in C3G treated groups (Fig. 10C).

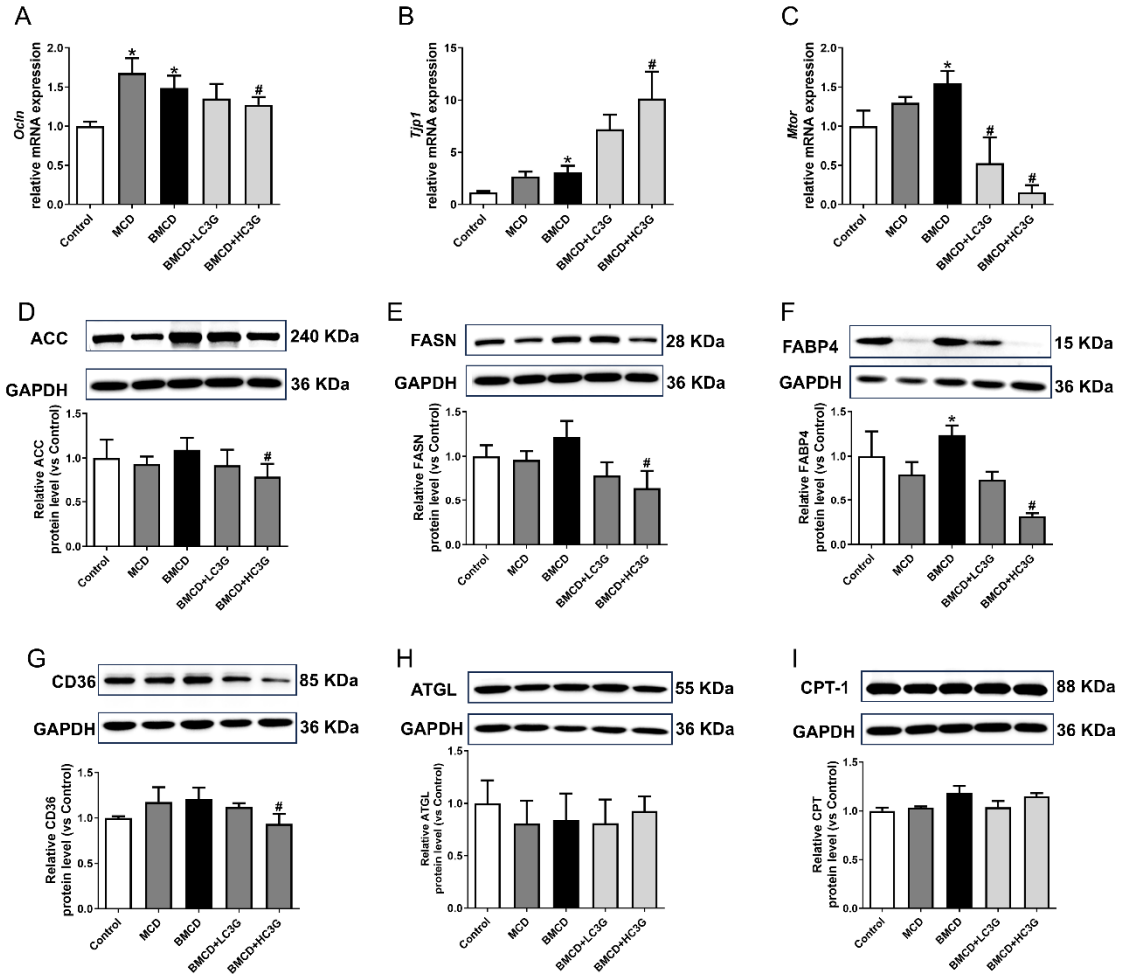

Fig. 10. C3G mediated the gene and protein expression related to lipid metabolism. Mitochondrial membrane potential was evaluated by JC-1 dye in isolated mitochondria (B). Bcl-2, Bax, GRP78, CHOP, and XBP-1 mRNA levels were measured by RT-qPCR (C-G). The results were expressed as mean ± SEM. When MCD group and BMCD group compared with control group, $^{*}P < 0.05$ was applied for the significant difference. When the BMCD+LC3G, BMCD+HC3G groups compared with BMCD group, $^{\#}P < 0.05$ showed the significant differences in groups.

The proteomic analysis revealed that C3G exhibit significant regulatory effects on lipid metabolism, particularly through modulation of key lipid-metabolizing enzymes. We further evaluated the crucial proteins related to lipid synthesis, transport and catabolism. ACC as the rate-limiting enzyme in fatty acid synthesis usually increased activity and gene expression in NAFLD. Our experimental data demonstrate that high-dose C3G intervention significantly suppressed ACC expression in the BMCD group, although no marked changes were observed in BMCD group (Fig. 10D). FASN another pivotal enzyme in lipogenesis, was also significantly inhibited at the protein level by C3G treatment (Fig. 10E). Furthermore, FABP4 as a crucial intracellular lipid chaperone involved in fatty acid transporting and metabolic regulation, showed remarkable downregulation following C3G administration (Fig. 10F). Intriguingly, our study revealed elevated FABP4 expression specifically in the BMCD group rather than the conventional MCD group, suggesting that AGEs generated during thermal processing might enhance lipogenesis through this pathway.

CD36, a fatty acid receptor responsible for fatty acid recognition and transmembrane transport, was found to undergo significant protein degradation in hepatic tissue following C3G intervention, which suggested decreased fatty acid translocation capacity into hepatocytes (Fig. 10G). Further investigation of lipid decomposition-associated enzymes was conducted (Fig. 10H&I). ATGL as a critical enzyme for triglyceride hydrolysis and fatty acid liberation, and carnitine CPT-1 as the rate-limiting enzyme in mitochondrial fatty acid β-oxidation, were analyzed. However, no significant differences in the expression levels of these lipolytic enzymes, and C3G administration did not induce observable regulatory effects on either enzyme. These findings collectively indicate that the regulatory effects of C3G on hepatic lipid accumulation in this model were found to be independent of lipid decomposition pathways.

4. Discussion

This study delineates a mechanism for C3G-mediated hepatoprotection. It had no effect on AGEs accumulation in liver but suppressed AGEs-RAGE signaling and downstream oxidative and inflammatory cascades. It could further protect mitochondrial and rough endoplasmic reticulum, and mediate lipogenic enzymes without affecting lipolysis pathways (Fig. 11).

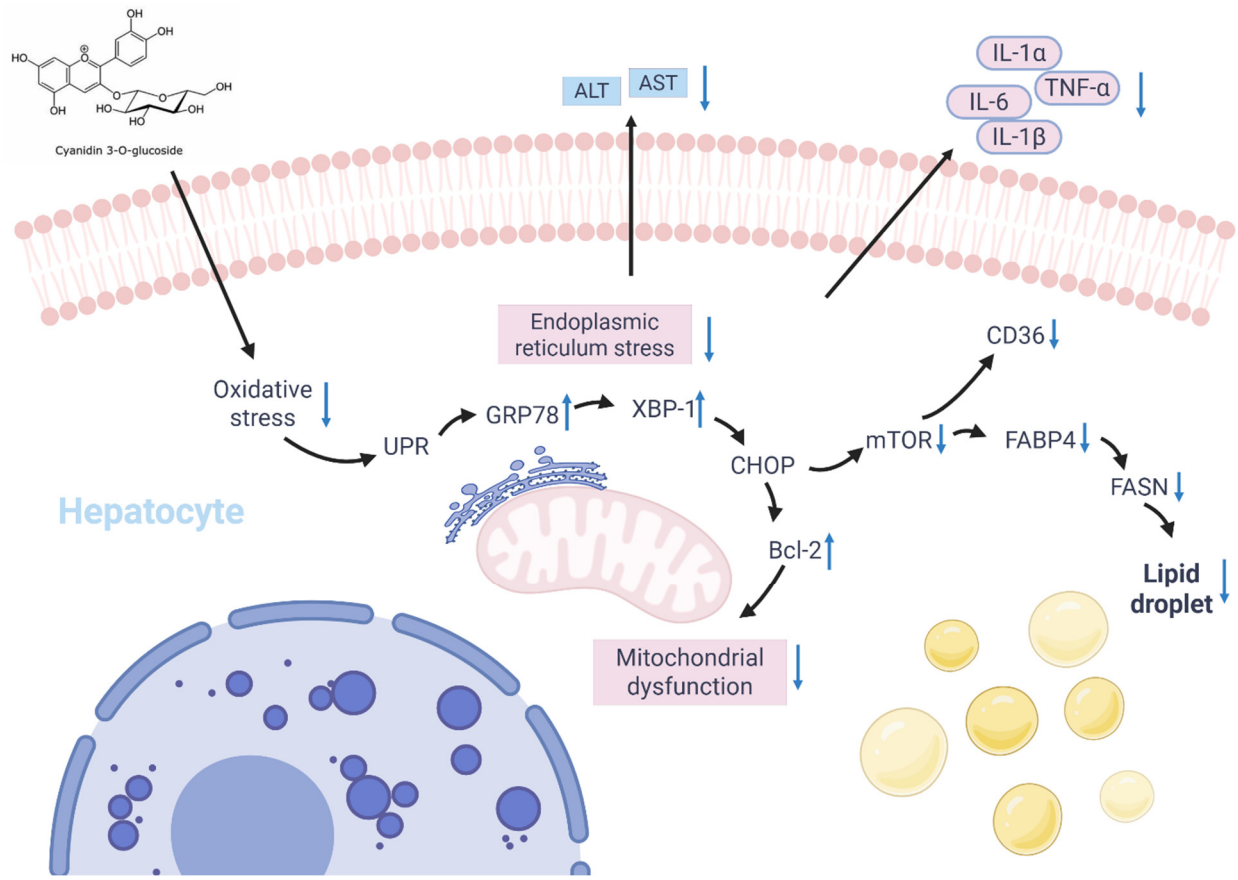

Fig. 11. Pathways related to the treatment of C3G on our NAFLD animal model.

The baking of the MCD diet established an MCD-AGEs model, that provides a unique platform for dissecting AGEs-specific contributions to NAFLD progression, circumventing metabolic confounders inherent to conventional models. Thermal cooking is a prevalent heat treatment method applied to food, resulting in the alteration of proteins, oxidation of fats, and the occurrence of Maillard reactions and caramelization[12]. These processes contribute to the creation of appealing flavors and colors. Nevertheless, certain compounds and nutrients that are sensitive to heat may break down, such as alkaloids, oxalates, tannins and phytates contents may respectively reduce 77%, 85%, 85%, and 86% in white cabbage[13]. While baking could also lead to the formation of harmful substances. Examples of these substances encompass heterocyclic aromatic amines, acrylamide, furan, polycyclic aromatic hydrocarbons, 5-hydroxymethylfurfural, acrolein, and AGEs[14]. After high temperature treatment, AGEs might rank first place to promote the liver injury in NAFLD. However, other pollutants formed during food thermal processing such as acrylamide and polyaromatic hydrocarbons (PAHs)[15]. Acrylamide could provoke NLRP3 inflammasome activation and MAPKs, NF-κB pathways to mediate inflammation and metabolic disorders in liver[16]. Multiple PAHs mixtures exposure to population may induce NAFLD by mediating HDL and TG in human metabolism[17].

AGEs could also be formed by non-enzymatic glycation reaction in diabetes, and elevate systemic ROS levels and impair antioxidant defenses. Conversely, oxidative stress exacerbates AGEs accumulation, establishing a pathogenic feedback loop. Both endogenous and exogenous AGEs are recognized as critical risk factors for diabetes progression[18]. Some studies have shown that high glucose level in the organism

could induce AGEs level at least 3 times higher than normal individuals in liver, kidney, lens and brain[19]. AGEs could exert deleterious effects on the disruption of cellular integrity, and impairment of organ function. The interaction between AGEs and their receptor RAGE triggers oxidative stress, inflammation, and fibrosis, thereby accelerating NAFLD. Emerging evidence suggests that NAFLD fibrogenesis is closely associated with dietary or metabolically derived AGEs[20, 21].

To elucidate the role of AGEs in NAFLD pathogenesis, the MCD diet model was employed. Unlike high-fat/high-sugar models, the MCD model avoids confounding effects of insulin resistance and hyperglycemia-induced endogenous AGEs, enabling isolated analysis of dietary AGEs. MCD feeding disrupts hepatic phosphatidylcholine synthesis by depriving methyl donors, impairing very-low-density lipoprotein assembly and triglyceride export[22]. Concurrently, elevated sucrose content promotes *de novo* lipogenesis, exacerbating hepatic steatosis, apoptosis, lipid peroxidation, and inflammation[23]. To enhance AGEs exposure, in BMCD group, the MCD diet was thermally processed, which amplified hepatic lipid accumulation and mortality. In our study, baking of the MCD diet induced more liver and body weight loss, which indicated more disturbance of energy supply, while C3G treatment showed no improvement on body or liver weight, which is consistent to the previous models that C3G could induce body and liver weight loss[21, 24].

H&E staining of the liver tissue revealed pronounced microvesicular steatosis, inflammatory infiltration, and necrosis in MCD and BMCD groups, confirming successful NAFLD induction. Notably, dietary supplementation with 60 mg/kg or 120 mg/kg C3G significantly reduced lipid vacuolization, ballooning, and inflammation, demonstrating its protective effects against AGEs-aggravated hepatic injury. The lipid droplet in BMCD group showed a little increase compared to the MCD group, but the lipid in the hepatocyte shows more microvesicular steatosis. C3G treatment reduced both macrovesicular and microvesicular steatosis. According to the findings in individuals with obesity, microvesicular steatosis is significantly associated with higher level of ALT, and with higher frequencies of hepatocellular ballooning, fibrosis, inflammation, and is considered as a reliable marker of NAFLD severity[25]. Although not much is known about the pathogenesis of microvesicular steatosis, in many cases the primary defect may be a mitochondrial lesion, and inhibition of mitochondrial fatty acid β-oxidation is the most commonly implicated defect[26].

Hepatic stellate cell (HSC) activation, driven by pro-inflammatory cytokines (TNF-α, MCP-1, IL-6, IL-1β), represents a pivotal mechanism in fibrogenesis. Activated HSCs transition from quiescent, lipid droplet-rich cells to myofibroblasts expressing α-smooth muscle actin (α-SMA) and desmin, secreting collagen I/III to promote fibrosis. Free fatty acids may be capable together with Toll like receptor ligands present in gut microbiota of activating inflammasomes and release IL-1α, IL-1β and IL-18 in hepatocytes[27]. IL-1 cytokine family are considered as pro-inflammatory members with prominent functions in regulating the cell proliferation, differentiation, and apoptosis in the liver. IL-1, IL-6 are increased in patients with NAFLD and correlate with systemic insulin resistance[28]. It is hypothesized that the increased IL-1 superfamily members and IL-6 are crucial to control IL-17 production and in differentiation of Th17 lymphocytes and

TGF-β, resulting in proinflammation and the activation of HSCs[29]. IL-17 is also a proinflammatory cytokine, in the pathogenesis of liver fibrosis, cirrhosis and autoimmune hepatitis. Elevated IL-17 in the circulation is also served as a clinical biomarker for predicting imminent hepatocellular carcinoma[30]. IL-10 could suppress the up-regulation of the HSCs activation and expression of α-smooth muscle actin. IL-10-deficient mice exhibited more severe liver fibrosis than wild-type mice[31]. TNF-α and MCP-1 are two crucial cytokines mediate the migration and activation of Kupffer cells and HSCs. In our study, IL-1α,β, IL-6, and TNF-α increased significantly in MCD, and with exacerbated inflammation in the BMCD, while C3G reduced these cytokine levels. IL-10 and IL-17A have not changed much, which may indicate an early stage of NASH, and liver fibrosis is not totally started. Although the model did not progress to NASH or fibrosis within the study, C3G intervention effectively mitigated cytokine release and improved survival outcomes.

Proteomic analysis revealed that MCD-induced NAFLD is mechanistically linked to mitochondrial impairment and ER stress. Efl1 is Elongation factor-like GTPase 1, involved in the biogenesis of the 60S ribosomal subunit and translational activation of ribosomes. Wars2 is a tryptophan--tRNA ligase in mitochondrial that activate and transfer the amino acids to their corresponding tRNAs during the translation of mitochondrial genes and protein synthesis. C3G administration ameliorated mitochondrial biosynthesis, electron transport chain efficiency, and membrane integrity, critical for energy metabolism and apoptosis regulation[32]. ER stress, triggered by lipotoxicity and glucotoxicity, disrupts VLDL trafficking and promotes hepatic lipid retention. Unfolded protein response (UPR) activation via the PERK/eIF2α/ATF4 axis upregulates VLDL receptor expression, exacerbating triglyceride accumulation. Conversely, PPARβ/δ and FGF21 activation attenuates steatosis by suppressing VLDLR[33]. Mitochondria-ER crosstalk, mediated by calcium flux and ROS exchange, amplifies cellular stress. Excessive fatty acid oxidation generates mitochondrial ROS, which disrupt ER redox balance and calcium homeostasis. Reciprocally, ER-derived calcium overload impairs mitochondrial membrane potential, further elevating ROS production and triggering cytochrome *C* release[34]. Oligosaccharyltransferase-48 (OST48), an ER-resident AGEs receptor, was implicated in AGEs-aggravated ER stress and hepatic fibrosis. Combined OST48 overexpression and dietary AGEs exposure synergistically promoted insulin resistance, hepatic glycogen accumulation, and oxidative stress, independent of steatosis[35].

In our study, the gene expression of *Bax* level of was not changed much, while *Bcl2* level increased in the BMCD group with significance. Additionally, C3G treatment with high dose dramatically induced the *Bcl2* gene expression. Bcl-2 family could mediate the outer mitochondrial membrane integrity and regulate the mitochondrial pathway of apoptosis. The balance of Bcl-2/Bax determines the dysfunction of mitochondrial, lead to the intermembrane proteins such as cytochrome *C* release, and promote the activation of caspase activation in the cytosol[36]. Additionally, GRP78 is a key regulator of liver inflammation and lipid metabolism, which locate in the transmembrane and could combine with unfolded protein to mediate p-ERK and XBP-1. p-ERK further induces the phosphorylation of Eif2α, that could elevate the level of CHOP to induce cell stress[37].

In the liver, ZO-1 and occludin are critical components of tight junctions that maintain the integrity of the blood-biliary barrier and regulate paracellular permeability in hepatocytes and bile duct epithelial cells. Their roles and interplay are pivotal in liver physiology and pathology, particularly in NAFLD[38]. *Mtor* is the gene mediate mTOR, which promotes *de novo* lipogenesis by upregulating sterol regulatory element-binding protein 1c (SREBP-1c), FASN and ACC[39]. ACC and FASN upregulation drive *de novo* synthesis of lipids, while CPT-1 inhibition limits β-oxidation, creating a lipid surplus. CD36/FABP4 overexpression enhances lipid uptake and intracellular transportation, further loading hepatocytes with FFAs. Impaired ATGL activity reduces lipolysis, trapping TGs in lipid droplets[40]. The accumulation of lipid is usually the outcome of the imbalance of lipid synthesis, transportation and oxidation. In our study, MCD and BMCD model have shown a little change in ACC, FASN, CD36, ATGL and CPT-1, but significantly upregulated FABP4. C3G significantly reduced the FABP4 level and inhibited CD36 level, which is consistent to the previous studies in some other models[41, 42].

5. Conclusion

This study primarily investigates the protective effects of anthocyanin intervention on hepatic injury in NAFLD mice exposed to AGEs. Our findings demonstrate that baked diet significantly exacerbated hepatic lipid accumulation in mice, while C3G intervention markedly inhibited hepatic steatosis and suppressed the release of inflammatory cytokines. These protective mechanisms may be partially attributed to the inhibition of AGEs-associated signaling pathways, as well as modulation of mitochondrial dysfunction and mitigation ER stress attenuation, which lead to suppression of lipid synthesis. These findings provide novel insights into the molecular pathways modulated by dietary anthocyanins, suggesting their therapeutic potential in ameliorating AGEs-associated metabolic dysregulation and NAFLD progression through multi-target interventions. Further investigations are warranted to elucidate the precise molecular cascades and translational implications of these observations, and the gut microbial metabolites the of C3G and the structure-activity relationship of different anthocyanins should be studied in the future for the better application.

Conflict of interest

The authors declare that the research was conducted in the absence of any commercial or financial relationships.

Data Availability

The data used to support the findings of this study are available from the corresponding author upon request.

Acknowledgements

This study is supported by the Special Fund Project for Science and Technology Innovation Strategy of Guangdong Province (2022B0202040001) and Natural Science Foundation of Guangzhou Municipality

(202201010504). The authors also thank for the National Natural Science Foundation of China (NSFC, No. 82204012, 81703211).

References

[1] X. Xu, K.L. Poulsen, L. Wu, et al., Targeted therapeutics and novel signaling pathways in non-alcohol-associated fatty liver/steatohepatitis (NAFL/NASH), Signal transduction and targeted therapy, 7 (2022) 287.

[2] L. Fan, W. Yu, B. Zhang, et al., Distinctive effects of different types of advanced glycation end-products (AGEs) on liver glucose metabolism, Food & Function, 13 (2022) 11298-11306.

[3] A. Twarda-Clapa, A. Olczak, A.M. Białkowska, et al., Advanced Glycation End-Products (AGEs): Formation, Chemistry, Classification, Receptors, and Diseases Related to AGEs, Cells, 11 (2022).

[4] J. Lu, M. Li, Y. Huang, et al., A comprehensive review of advanced glycosylation end products and N- Nitrosamines in thermally processed meat products, Food Control, 131 (2022) 108449.

[5] A. Sakasai-Sakai, K. Takeda, M. Takeuchi, Involvement of Intracellular TAGE and the TAGE-RAGE-ROS Axis in the Onset and Progression of NAFLD/NASH, Antioxidants (Basel, Switzerland), 12 (2023).

[6] M. Liu, S. Li, M. Guan, et al., Leptin pathway is a crucial target for anthocyanins to protect against metabolic syndrome, Crit Rev Food Sci Nutr, 65 (2025) 2046-2061.

[7] N. Randeni, J. Luo, B. Xu, Critical Review on Anti-Obesity Effects of Anthocyanins Through PI3K/Akt Signaling Pathways, Nutrients, 17 (2025).

[8] D.Z. Oumeddour, S. Al-Dalali, L. Zhao, et al., Recent advances on cyanidin-3-O-glucoside in preventing obesity-related metabolic disorders: A comprehensive review, Biochemical and biophysical research communications, 729 (2024) 150344.

[9] X. Jiang, X. Li, W. Feng, et al., Baking of methionine-choline deficient diet aggravates testis injury in mice, Food Chem Toxicol, 154 (2021) 112245.

[10] X. Jiang, C. Zhu, X. Li, et al., Cyanidin-3- O-glucoside at Low Doses Protected against 3-Chloro-1,2-propanediol Induced Testis Injury and Improved Spermatogenesis in Male Rats, Journal of agricultural and food chemistry, 66 (2018) 12675-12684.

[11] E.M. Brunt, D.E. Kleiner, L.A. Wilson, et al., Nonalcoholic fatty liver disease (NAFLD) activity score and the histopathologic diagnosis in NAFLD: distinct clinicopathologic meanings, Hepatology, 53 (2011) 810-820.

[12] L. Zhao, J. Wang, P. Yang, et al., Exploring relationships between precursor changes and aroma-active compounds formation of cooked Tibetan pork under different cooking methods, Meat science, 225 (2025) 109819.

[13] M. Waseem, S. Akhtar, M. Qamar, et al., Effect of Thermal and Non-Thermal Processing on Nutritional, Functional, Safety Characteristics and Sensory Quality of White Cabbage Powder, Foods (Basel, Switzerland), 11 (2022).

[14] H. Hu, Y. Wang, M. Shen, et al., Effects of baking factors and recipes on the quality of butter cookies and the formation of advanced glycation end products (AGEs) and 5-hydroxymethylfurfural (HMF), Current research in food science, 5 (2022) 940-948.

[15] H. Yazdanpanah, F. Kobarfard, C. Tsitsimpikou, et al., Health risk assessment of process-related contaminants in bread, Food Chem Toxicol, 170 (2022) 113482.

[16] D. Kathuria, Hamid, S. Gautam, et al., Maillard reaction in different food products: Effect on product quality, human health and mitigation strategies, Food Control, 153 (2023) 109911.

[17] Z. Hu, Y. Li, Y. Yang, et al., Serum lipids mediate the relationship of multiple polyaromatic hydrocarbons on non-alcoholic fatty liver disease: A population-based study, The Science of the total environment, 780 (2021) 146563.

[18] M. Khalid, A. Adem, The dynamic roles of advanced glycation end products, Vitamins and hormones, 125 (2024) 1-29.

[19] B.H. Lee, W.H. Hsu, Y.W. Hsu, et al., Dimerumic acid attenuates receptor for advanced glycation endproducts signal to inhibit inflammation and diabetes mediated by Nrf2 activation and promotes methylglyoxal metabolism into d-lactic acid, Free radical biology & medicine, 60 (2013) 7-16.

[20] S. Corrao, L. Calvo, W. Granà, et al., Metabolic dysfunction-associated steatotic liver disease: A pathophysiology and clinical framework to face the present and the future, Nutrition, metabolism, and cardiovascular diseases : NMCD, 35 (2025) 103702.

[21] F. Xie, J. Zhao, D. Liu, et al., Associations of dietary advanced glycation end products with liver steatosis via vibration controlled transient elastography in the United States: a nationwide cross-sectional study, European journal of nutrition, 63 (2024) 173-183.

[22] M.K. Pickens, J.S. Yan, R.K. Ng, et al., Dietary sucrose is essential to the development of liver injury in the methionine-choline-deficient model of steatohepatitis, Journal of lipid research, 50 (2009) 2072-2082.

[23] S.H. Zeisel, Choline: critical role during fetal development and dietary requirements in adults, Annual Review of Nutrition, 26 (2006) 229-250.

[24] Z. Chen, C. Wang, Y. Pan, et al., Hypoglycemic and hypolipidemic effects of anthocyanins extract from black soybean seed coat in high fat diet and streptozotocin-induced diabetic mice, Food & function, 9 (2018) 426-439.

[25] C.W. Germano, P.F. Mega, T.J.A.P. Mattosinho, et al., Microvesicular Steatosis in Individuals with Obesity: a Histological Marker of Non-alcoholic Fatty Liver Disease Severity, Obesity Surgery, 33 (2023) 813-820.

[26] A.B. Koenig, A. Tan, H. Abdelaal, et al., Review article: Hepatic steatosis and its associations with acute and chronic liver diseases, Alimentary pharmacology & therapeutics, 60 (2024) 167-200.

[27] L. Barbier, M. Ferhat, E. Salamé, et al., Interleukin-1 Family Cytokines: Keystones in Liver Inflammatory Diseases, Frontiers in immunology, 10 (2019) 2014.

[28] M. Praktiknjo, R. Schierwagen, S. Monteiro, et al., Hepatic inflammasome activation as origin of Interleukin-1α and Interleukin-1β in liver cirrhosis, Gut, 70 (2021) 1799-1800.

[29] T.G. Simon, M.E.P. Trejo, R. McClelland, et al., Circulating Interleukin-6 is a biomarker for coronary atherosclerosis in nonalcoholic fatty liver disease: Results from the Multi-Ethnic Study of Atherosclerosis, International journal of cardiology, 259 (2018) 198-204.

[30] Z. Chen, C. Ding, K. Chen, et al., Investigating the causal association between obesity and risk of hepatocellular carcinoma and underlying mechanisms, Scientific reports, 14 (2024) 15717.

[31] H.T. Nga, J.S. Moon, J. Tian, et al., Interleukin-10 Attenuates Liver Fibrosis Exacerbated by Thermoneutrality, Frontiers in medicine, 8 (2021) 672658.

[32] T. Xilan, S. Tianran, J. Xinwei, et al., Purified anthocyanins from bilberry and black currant attenuate hepatic mitochondrial dysfunction and steatohepatitis in mice with methionine and choline deficiency, Journal of Agricultural & Food Chemistry, 63 (2015) 552-561.

[33] K. Zhang, S. Wang, J. Malhotra, et al., The unfolded protein response transducer IRE1α prevents ER stress-induced hepatic steatosis, The EMBO Journal, 30 (2011) 1357-1375.

[34] R. Ghemrawi, S.F. Battaglia-Hsu, C. Arnold, Endoplasmic Reticulum Stress in Metabolic Disorders, Cells, 7 (2018).

[35] A. Zhuang, F.Y. Yap, C. Bruce, et al., Increased liver AGEs induce hepatic injury mediated through an OST48 pathway, Sci Rep, 7 (2017) 12292.

[36] J.-C. Martinou, Richard J. Youle, Mitochondria in Apoptosis: Bcl-2 Family Members and Mitochondrial Dynamics, Developmental Cell, 21 (2011) 92-101.

[37] H. Liu, X. Zhang, S. Zhang, et al., Oxidative Stress Mediates Microcystin-LR-Induced Endoplasmic Reticulum Stress and Autophagy in KK-1 Cells and C57BL/6 Mice Ovaries, Front Physiol, 9 (2018) 1058-1058.

[38] N.P. Lee, J.M. Luk, Hepatic tight junctions: from viral entry to cancer metastasis, World journal of gastroenterology, 16 (2010) 289-295.

[39] Q. Ren, Q. Sun, J. Fu, Dysfunction of autophagy in high-fat diet-induced non-alcoholic fatty liver disease, Autophagy, 20 (2024) 221-241.

[40] J. Li, C. Li, X. Wu, et al., Protocatechuic Acid Suppresses Lipid Uptake and Synthesis through the PPARγ Pathway in High-Fat Diet-Induced NAFLD Mice, Journal of agricultural and food chemistry, 73 (2025) 4012-4026.

[41] L. Saulite, K. Jekabsons, M. Klavins, et al., Effects of malvidin, cyanidin and delphinidin on human adipose mesenchymal stem cell differentiation into adipocytes, chondrocytes and osteocytes, Phytomedicine : international journal of phytotherapy and phytopharmacology, 53 (2019) 86-95.

[42] Y.P. Lu, X.H. Wang, B. Xia, et al., C3G improves lipid droplet accumulation in the proximal tubules of high-fat diet-induced ORG mice, Pharmacological research, 211 (2025) 107550.